JMEPEG (2019) 28:5361–5368
https://doi.org/10.1007/s11665-019-04282-x

1059-9495/$19.00

High-Carbon Ferrochrome Effects on Microstructure and Mechanical Properties of Powder Metallurgy Titanium Alloys

Boxin Lu, Ce Zhang, Zhimeng Guo, Fang Yang, Haiying Wang, AlexA. Volinsky, and Li You

(Submitted April 2, 2018; in revised form August 8, 2019; published online August 28, 2019)

In this paper, the powder metallurgy method was employed to prepare titanium alloys with high-carbon ferrochrome (HCFeCr). With the HCFeCr addition, the size of the β grains decreased and the lamellae of the α phase became thinner. The TiC strengthening phase precipitated at the grain boundaries, resulting in the inhibition of the β grain growth and hardness enhancement. In addition, Fe and Cr as β-stabilizing elements existed in the enriched β-Ti phase, which increased the β phase amount. The strength improvement was attributed to grain size optimization and strengthening phase formation. With the 9 wt.% HCFeCr addition, the corresponding Vickers hardness increased to 480 HV, which is 60% higher than the Ti6Al4V alloy. The tensile and yield strength was 1228 and 1140 MPa, respectively. The addition of HCFeCr can effectively enhance the strength and hardness while reducing the cost. This is a promising additive to obtain low-cost Ti alloys with high mechanical properties.

Keywords carbon titanium, high-carbon ferrochrome, mechanical properties, powder metallurgy, titanium alloy

1. Introduction

Titanium and titanium alloys are important high-quality light structural and functional metals. They are used in aerospace, military, and medical applications because of their excellent mechanical properties and corrosion resistance (Ref 1, 2). However, industrial applications of titanium and titanium alloys are greatly restricted due to the high cost (Ref 3, 4). The high cost of titanium products has many reasons. On the one hand, the molten Ti exhibits an extremely high chemical activity, so it will react with most gases and crucible materials. Thus, conventional casting methods require special production equipment (Ref 5, 6). On the other hand, the processing cost is high because of the poor machinability associated with a relatively low thermal conductivity of titanium alloys (Ref 7, 8). The material utilization is only 10% for some complex shape parts. To reduce the cost of titanium products, many researchers have focused on the powder metallurgy (PM) technology. Due to its near-net-shape capabilities, homogenous microstructure, and isotropic properties, PM technology is considered as an effective approach to obtain low-cost Ti alloys (Ref 9–11).

The advantages of PM Ti alloys include many aspects. First, the sintering temperature of PM titanium alloys is lower than the melting point of titanium, so they can be processed without melting titanium. Second, the near-net forming PM process can reduce the cutting cost. PM titanium alloys also have uniform composition without components segregation. Finally, the dispersion strengthening phases in PM Ti alloys can be beneficial to enhance the mechanical properties (Ref 12, 13). Therefore, the prospects of PM Ti alloys are very broad. The commonly used commercial Ti alloy is Ti6Al4V grade 5 with an expensive V element addition. Many efforts have been made recently to prepare low-cost titanium alloys by adding inexpensive alloying elements, such as Fe, Mn, and Si (Ref 14, 15). Among various elements, Fe is regarded as the most promising due to its low cost. The tensile strength dramatically improves with the Fe addition (Ref 16). One of the limitations of Fe in ingot metallurgy Ti alloys is the elements' segregation because of the density difference. This problem can be effectively avoided by using PM methods.

Previous research has shown that Cr is a stabilizing element for the β-Ti phase and has good solubility in it (Ref 17). Generally, C is a common impurity element in Ti alloys, but titanium carbide (TiC) particles can be synthesized in situ, enhancing the alloy hardness and strength (Ref 18–20). Therefore, high-carbon ferrochrome (HCFeCr) was chosen as an addition to pure Ti in this article. HCFeCr contains Fe and Cr elements; it is less expensive and easier to obtain. It is also expected to further improve the mechanical properties of the titanium alloy with carbon introduction.

The PM method was used to prepare Ti alloys to avoid Fe and Cr elements segregation. In addition, the effects of HCFeCr on microstructure and mechanical properties of PM titanium alloy were investigated. For comparison, the commercial Ti6Al4V alloy was also prepared. To date, there have been no related reports in this field.

Boxin Lu, Ce Zhang, Zhimeng Guo, Fang Yang, and **Haiying Wang**, Institute for Advanced Materials and Technology, University of Science and Technology Beijing, Beijing 100083, China; **Alex A. Volinsky**, Department of Mechanical Engineering, University of South Florida, Tampa, FL 33620; and **Li You**, State Key Laboratory for Advanced Metals and Materials, University of Science and Technology Beijing, Beijing 100083, China. Contact e-mails: yangfang@ustb.edu.cn, volinsky@usf.edu, and youli-0104321@163.com.

2. Experimental Procedure

2.1 Alloy Preparation

The raw materials were hydrogenation–dehydrogenation (HDH) Ti powder (99.5% purity, D_{50} = 10 μm), Ti6Al4V powder (99.5% purity, D_{50} = 10 μm), and HCFeCr powder (99.9% purity, D_{50} = 20 μm). Chemical analysis results of the raw powder are listed in Table 1. The HDH titanium and the Ti6Al4V powder size is about 10 μm, and the HCFeCr powder size is about 20 μm, as shown in Fig. 1.

The HDH Ti powder was mixed with various amounts of the HCFeCr powder (3, 5, 7, 9, and 11 wt.%). The powder was mixed by ball milling for 2 h using a SPEX 8000 mixer/mill. The weight ratio of the balls to the raw material was 5:1. Then, the mixed powder was uniaxially cold-pressed (zinc stearate lubricated floating die) with 700 MPa pressure. The compact size was about 15 mm × 15 mm × 120 mm. The sintering was carried out at 1573 K for 1 h in a high-vacuum atmosphere (10^{-3} Pa) using the 5 K/min heating and cooling rate. The sintering temperature was referenced to the temperature of titanium alloying and the temperature at which TiC forms (Ref 21). The Ti6Al4V powder was pressed and sintered using the same processing parameters as the comparison group.

2.2 Testing and Characterization

The specimens for mechanical properties analysis were prepared as described in the ASTM E8 standard (Ref 22). The dimensions in millimeters of the tensile test specimen are shown in Fig. 2. Five samples for each processing condition were tested to confirm reproducibility. Tensile properties of the specimens were tested by an electronic universal testing machine (Instron 6025). The Vickers hardness (HV30) was measured using a universal tester (Wilson Wolpert). The phases composition was analyzed by x-ray diffraction (XRD) using the Shimadzu XRD-6000 diffractometer with Cu Kα radiation operating at 40 kV and 40 mA between 20° and 90° 2θ angle range. The microstructure of the sintered samples was characterized by scanning electron microscope (Philips LEO-1450) equipped with the Oxford Instruments X-Max 80 energy-dispersive x-ray spectroscopy (EDS) detector. The EDS analysis was performed to evaluate the uniformity of different elements distribution and to validate the effectiveness of the PM process in homogenizing the elements during sintering.

Table 1 Chemical composition of raw powders in wt.%

	Al	V	Fe	Cr	C	O	Ti
Ti	…	…	0.3	…	0.06	0.35	Bal.
Ti6Al4V	6.3	4.3	0.25	…	0.06	0.35	Bal.
HCFeCr	…	…	Bal.	60	8	0.5	…

3. Results and Discussion

3.1 Microstructure Characterization

Figure 3 shows the microstructure of the sintered Ti-HCFeCr and Ti6Al4V alloys. The sintered alloys have a typical

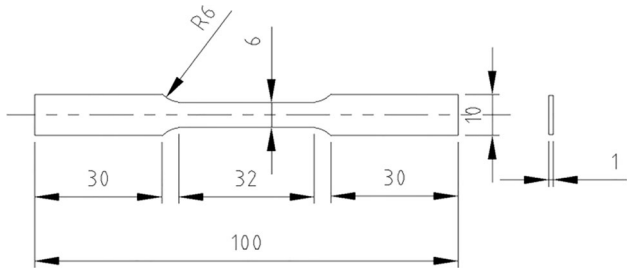

Fig. 2 Sample dimensions in millimeters for the tensile test

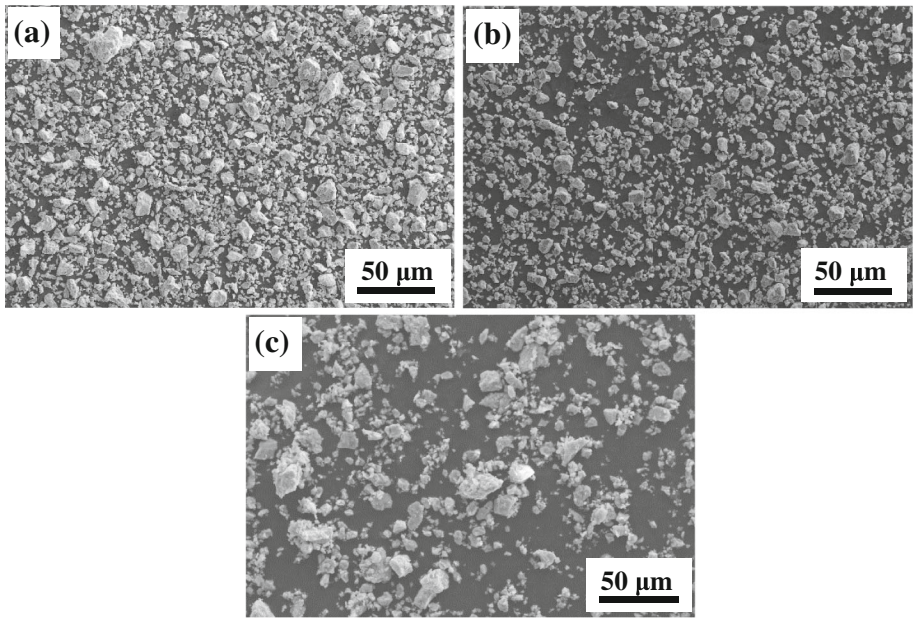

Fig. 1 SEM micrographs of the raw materials: (a) HDH Ti powder, (b) Ti6Al4V powder, (c) high-carbon ferrochrome powder

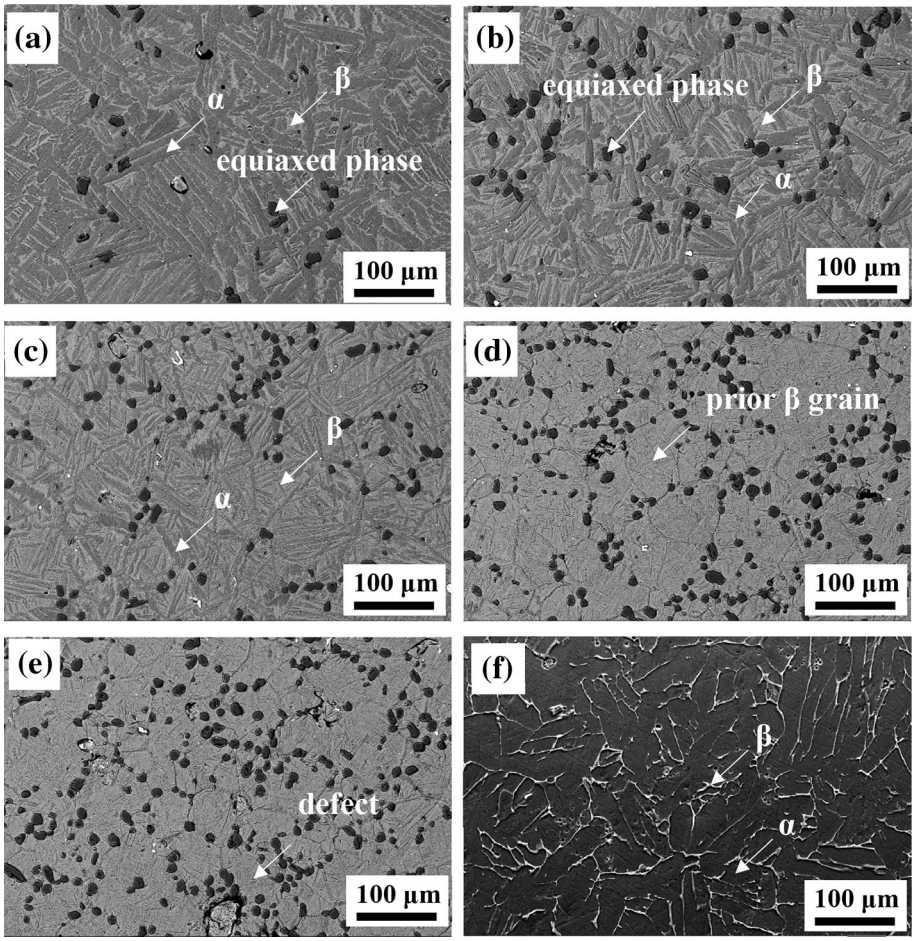

Fig. 3 SEM micrographs of the sintered samples: (a) Ti-3 HCFeCr, (b) Ti-5 HCFeCr, (c) Ti-7 HCFeCr, (d) Ti-9 HCFeCr, (e) Ti-11 HCFeCr, (f) Ti6Al4V

α–β lamellar structure. As shown in Fig. 3(a), the Ti-3HCFeCr sample has alpha lamellae with 20 μm width and the prior beta phase grain size of over 200 μm. This is a common structure of titanium alloys slowly cooled from the beta region (Ref 23). The width of the alpha lamellae and the beta grain size gradually decreased with higher Fe and Cr content. For the Ti-7HCFeCr sample in Fig. 3(c), the width of the alpha lamellae changed to 10 μm. After adding 9 and 11 wt.% HCFeCr, the β grain boundaries can be clearly seen and the prior β grain size was about 50 and 30 μm. However, there were also a few defects in Fig. 3(e).

In addition, it can be observed that the equiaxed phase, corresponding to the dark contrast region, formed in the matrix for each sample. As shown in Fig. 3, the average diameter of the equiaxed phase is about 10-15 μm. The proportion of the equiaxed phase increased with the HCFeCr content. In Fig. 3(d), the equiaxed phase formed at the grain boundaries, which prevented the matrix grain growth.

Figure 4 and Table 2 show the results of EDS analysis of different regions in the Ti-3HCFeCr sample. The dark phase, "point 2" in Fig. 4, only contained Ti and C elements. Therefore, it can be inferred that the equiaxed phase was the TiC phase. There were almost no Fe and Cr in the α phase ("point 3"). The EDS analysis revealed that Fe and Cr were mainly distributed in the β phase ("point 1"), as given in Table 2. This is expected because both Cr and Fe have a higher solubility in the beta phase. Based on the Ti-Fe and Ti-Cr binary phase diagrams, Fe and Cr are barely soluble in the α phase (Ref 24).

Figure 5 shows the distribution of different elements in the Ti-3HCFeCr alloy. The introduced Fe and Cr elements were evenly distributed in the beta phase, and there was no obvious segregation. This was mainly due to the application of PM technology. Fine raw material powder was uniformity mixed after a long time of ball milling. In the sintering process, the composition homogenization depends largely on the diffusion of Fe and Cr. Because the diffusion coefficients of Fe and Cr in titanium are relatively high, it was also beneficial for the homogenization of the alloying elements (Ref 25, 26).

The composition of the precipitated phase was further analyzed by XRD. As shown in Fig. 6, the main phases are Ti and TiC. Thus, it is clarified that the equiaxed phase is the TiC phase. The corresponding carbon content increased with more high-carbon ferrochromium, resulting in a larger amount of the TiC phase precipitation (Ref 27). This is also consistent with the SEM results.

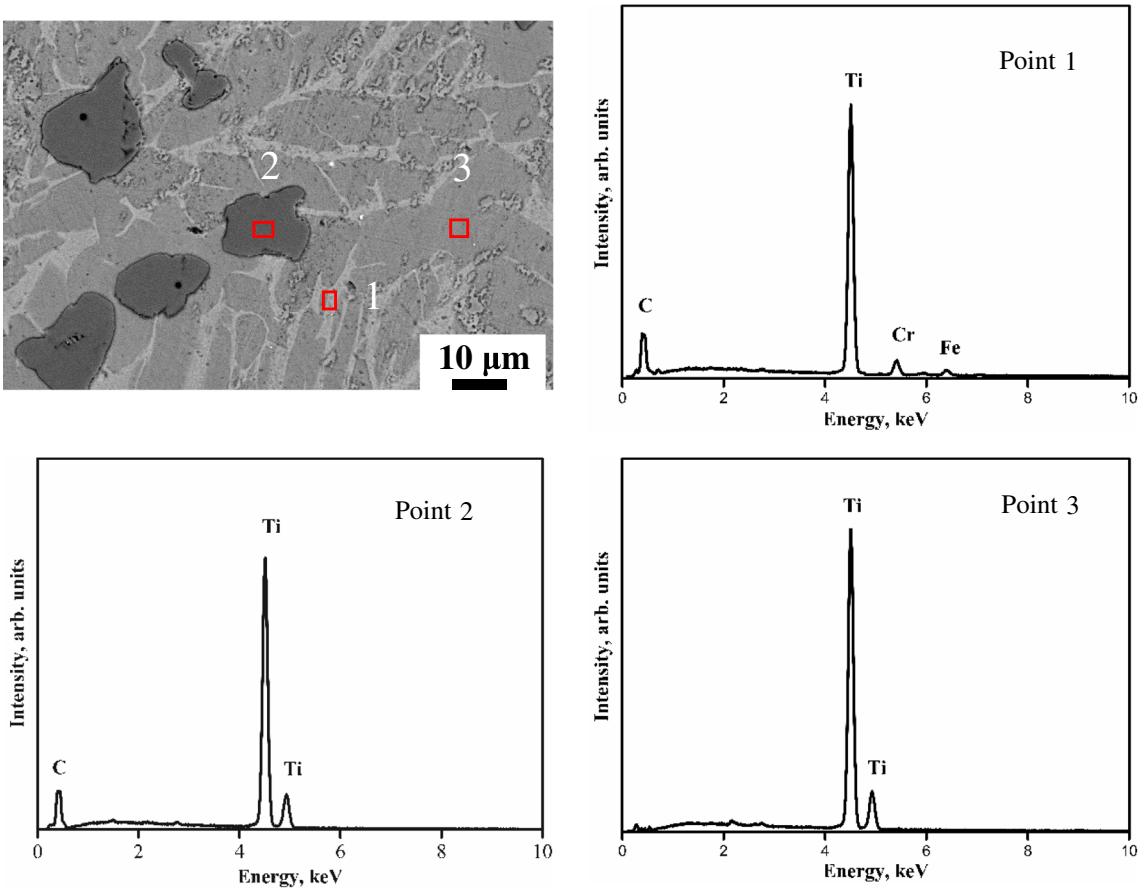

Fig. 4 EDS analysis of the Ti-3HCFeCr alloy

Table 2 Results of the Ti-3HCFeCr EDS analysis in wt.%

	C	Ti	Fe	Cr
Point 1	0.43	88.47	3.68	7.42
Point 2	3.45	96.55	0	0
Point 3	0	99.66	0	0.34

Based on the phase diagrams, Fe and Cr can form intermetallic compounds with titanium, which will affect mechanical properties (Ref 24). However, it was found that these compounds did not appear for the current quantity and process conditions, as shown in Fig. 6. This is mainly because the rates of eutectoid reactions of Fe-Ti and Cr-Ti are relatively slow. There were no intermetallic compounds formed at the current cooling rate.

As shown in Fig. 6, the Ti-HCFeCr alloys all have hexagonal alpha titanium phase and body-centered cubic beta titanium phase. The diffraction reflection intensity of the (101) planes of the alpha Ti phase was reduced with higher HCFeCr content, while it increased for the (100) planes of the beta Ti phase. These results indicated that the higher the content of beta stabilizers, the greater the relative amount of the beta phase present in the microstructure, which is consistent with the SEM results.

In order to evaluate the mechanical properties of the Ti-HCFeCr alloys, the tensile tests were carried out. The results were compared with the PM Ti6Al4V and cast Ti6Al4V (values of ASTM standard). From the stress–strain curves reported in Fig. 7, the ultimate tensile strength (UTS) of the Ti-HCFeCr alloys was significantly increased compared with the PM Ti6Al4V alloy. As given in Table 3, the cast Ti6Al4V and the PM Ti6Al4V alloys had UTS of 825 and 892 MPa, while the Ti-3HCFeCr sample was higher at 923 MPa. Meanwhile, with the addition of high-carbon ferrochromium, the tensile strength and yield strength (YS) increased. When 9% HCFeCr was added, UTS was 1228 MPa and YS was 1140 MPa. The main reason for improving the strength is the solid solution strengthening effect of Fe and Cr. After adding Fe and Cr β-stabilizing elements, the beta phase is more stable and the tendency to decompose decreases during cooling. Due to the beta phase having higher strength, a

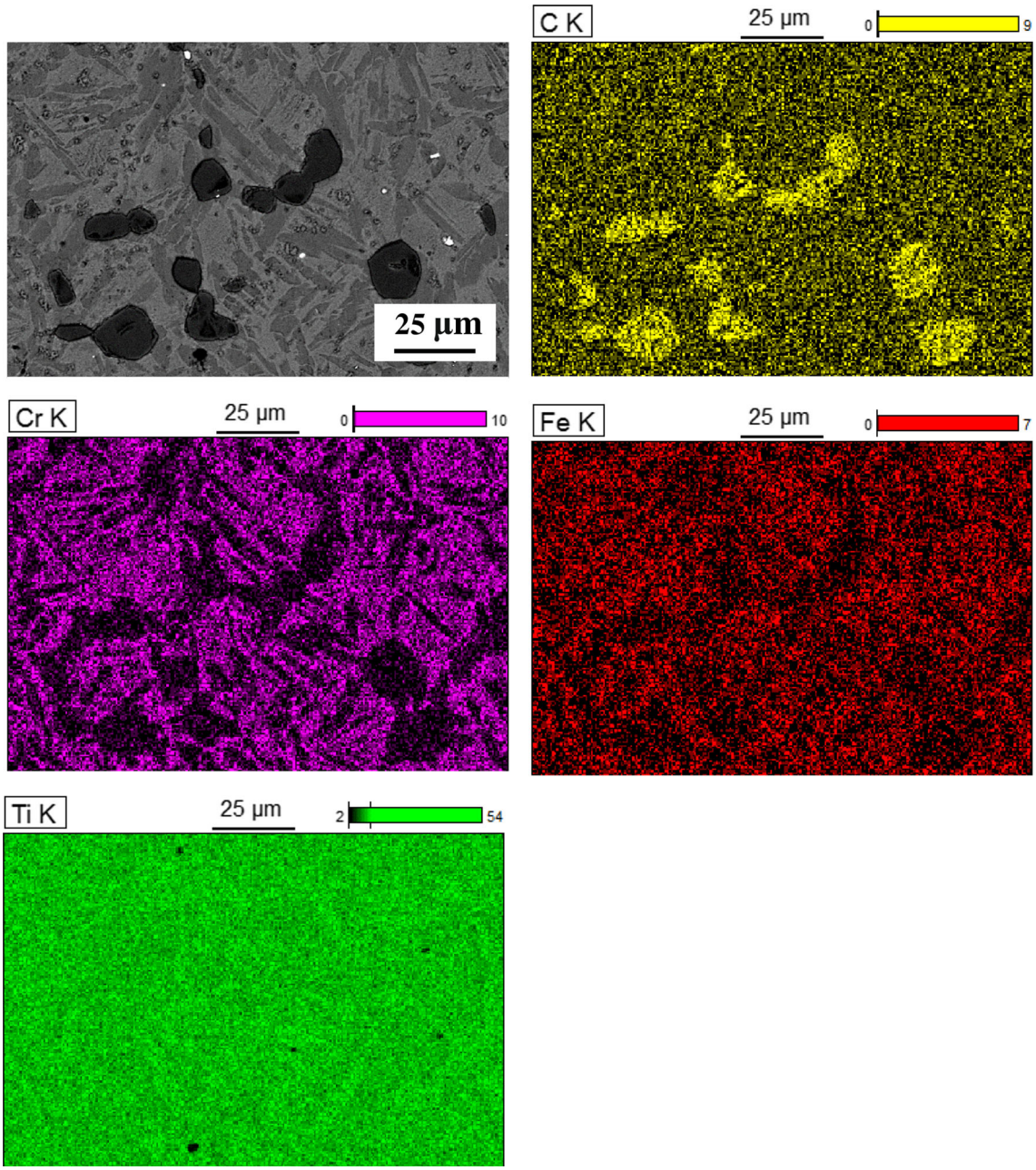

Fig. 5 EDS analysis of the Ti-7HCFeCr sample showing Ti, Cr, Fe, and C elements distribution

larger amount of the beta phase resulted in higher alloy tensile strength. On the other hand, the elongation (EL) decreased with the HCFeCr content, as given in Table 3. The EL of cast and PM Ti6Al4V is 6% and 6.9%, respectively, while it is 3.1% for the Ti-9HCFeCr alloy. The main reason is the formation of the brittle TiC phase, which causes plasticity reduction. The Ti-9HCFeCr sample has good UTS (1228 MPa), YS (1140 MPa) and EL (3.1%). This can also be attributed to the formation of the TiC phase (Ref 28). The TiC phase not only increased the strength but also prevented grain growth and refined the β grains, resulting in mechanical properties optimization.

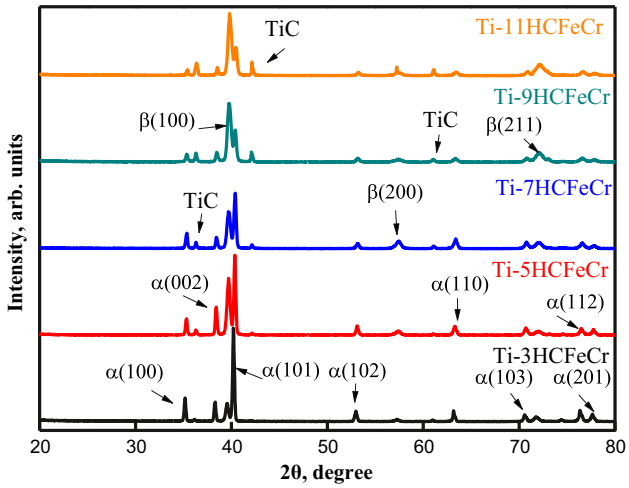

Fig. 6 X-ray diffraction patterns of the Ti-HCFeCr alloys

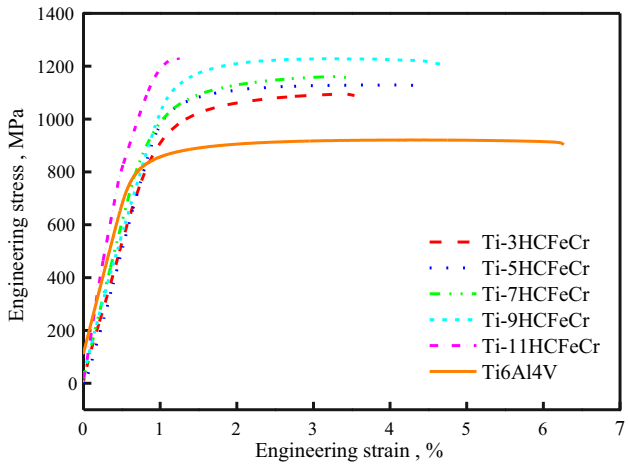

Fig. 7 Stress–strain curves of the Ti-HCFeCr and Ti6Al4V alloys

Table 3 Tensile properties of the Ti-HCFeCr and Ti6Al4V alloys

Sample	UTS, MPa	YS, MPa	EL, %
Ti-3HCFeCr	923 ± 3	867 ± 2	4.4 ± 0.1
Ti-5HCFeCr	1103 ± 4	1028 ± 3	3.5 ± 0.3
Ti-7HCFeCr	1154 ± 2	1081 ± 1	3.2 ± 0.2
Ti-9HCFeCr	1228 ± 2	1140 ± 2	3.1 ± 0.1
Ti-11HCFeCr	1233 ± 4	1120 ± 10	1.2 ± 0.5
PM Ti6Al4V	892 ± 3	845 ± 1	6.9 ± 0.3
Cast Ti6Al4V Ref 29	895	825	6

When the HCFeCr content reached 11 wt.%, it can be seen that the elongation decreased and the performance was no longer stable. By observing the fracture morphology in Fig. 8, when the content of HCFeCr was 3-9 wt.%, the fracture morphology was mainly ductile fracture. When the content of HCFeCr was 11 wt.%, the fracture surface exhibited obvious cleavage fracture. The microstructure in Fig. 3(e) shows a large amount of TiC in the Ti-11HCFeCr sample. Too much TiC hindered sintering and produced many defects. Thus, the elongation of the Ti-11HCFeCr sample was only 1.2%. To sum up, the Ti-9HCFeCr sample has the best mechanical properties.

To evaluate the effects of HCFeCr, the hardness of the samples was tested. Figure 9 shows Vickers hardness of the Ti-HCFeCr alloys as a function of the HCFeCr content, along with the hardness of cast and PM Ti6Al4V alloys. With the addition of HCFeCr, the hardness of the Ti-HCFeCr alloys is significantly increased compared to Ti6Al4V. With the 3 wt.% HCFeCr addition, the hardness was 400 HV, much higher than the cast and PM Ti6Al4V alloys (368 HV and 300 HV) (Ref 29). With higher HCFeCr content, the hardness gradually increased to 500 HV. Compared with the Ti-3HCFeCr, the hardness of the Ti-11HCFeCr alloy increased from 400 HV to 500 HV. The increase in hardness was caused by the increase in the volume fraction of titanium carbide and grain refinement. However, further research is needed to determine which factor plays the major role.

4. Conclusions

In this paper, a low-cost titanium alloy was prepared by the powder manufacturing technology. During the PM process, vanadium was replaced by HCFeCr. The performance of low-cost titanium alloys with different HCFeCr contents was investigated, and the following conclusions can be drawn:

1. With the HCFeCr addition, the prior β grain size decreased and the α phase became thinner and shorter. The prior β grain size was over 200 μm and the width of α lamellae was about 20 μm in the Ti-3HCFeCr sample. After adding 9 wt.% HCFeCr, the prior β grain size was about 50 μm and the width of the α lamellae was less than 10 μm. The equiaxed TiC phase precipitated at grain boundaries. The size of TiC was about 10-15 μm.

2. Compared with the Ti6Al4V alloy, the tensile strength and yield strength of the Ti-HCFeCr alloy have been greatly increased. With the 9 wt.% HCFeCr addition, the UTS is 1228 MPa and the YS is 1140 MPa. In addition, the elongation is 3.1% and the Vickers hardness can reach 480 HV. Thus, the optimal content of the HCFeCr powder added into the titanium alloys is 9 wt.%.

3. It is feasible to use low-cost HCFeCr as a source of alloying elements in Ti alloys. Thus, production costs can be effectively controlled.

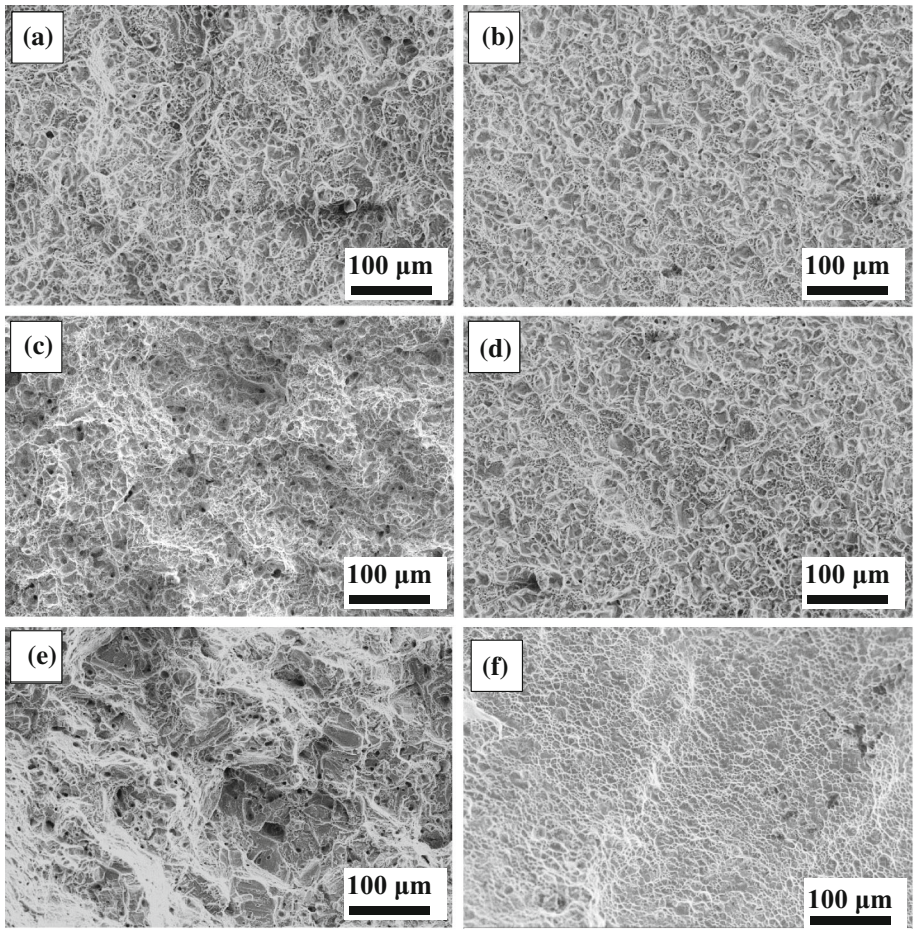

Fig. 8 Fracture morphology of the sintered samples: (a) Ti-3 HCFeCr, (b) Ti-5 HCFeCr, (c) Ti-7 HCFeCr, (d) Ti-9 HCFeCr, (e) Ti-11 HCFeCr, (f) PM Ti6Al4V

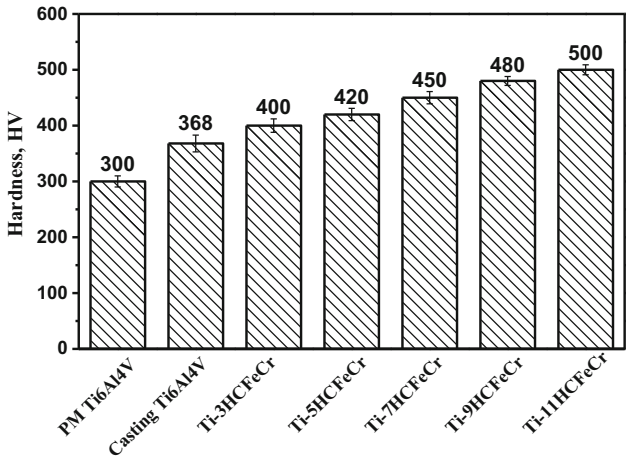

Fig. 9 Vickers hardness of the Ti-HCFeCr and Ti6Al4V alloys

Acknowledgments

This work was supported by the State Key Lab of Advanced Metals and Materials (No. 2018-Z06). AV acknowledges support from the National Science Foundation (IRES 1358088).

References

1. C. Leyens and M. Peters, *Titanium and Titanium Alloys: Fundamentals and Applications*, Wiley-YCH, Hoboken, 2003
2. D. Banerjee and J.C. Williams, Perspectives on Titanium Science and Technology, *Acta Mater.*, 2013, **61**(3), p 844–879
3. F.H.S. Froes, M.N. Gungor, and M.A. Imam, Cost-Affordable Titanium: the Component Fabrication Perspective, *JOM*, 2007, **59**(6), p 28–31
4. M.A. Imam, F.H. Froes, and R.G. Reddy, Research and Development of low-Cost Titanium Alloys for Biomedical Applications, *Key Eng. Mater.*, 2013, **551**, p 133–139
5. R. Zhang, D.J. Wang, S.Q. Liu, H.S. Ding, and S.J. Yuan, Hot Deformation Characterization of Lamellar Ti-43Al-2Si Alloy Fabricated By Cold Crucible Continuous Casting, *J. Alloys Compd.*, 2016, **688**, p 542–552
6. S. Schafföner, C.G. Aneziris, H. Berek, J. Hubálková, B. Rotmann, and B. Friedrich, Corrosion Behavior of Calcium Zirconate Refractories in Contact with Titanium Aluminide Melts, *J. Eur. Ceram. Soc.*, 2015, **35**(3), p 1097–1106
7. K. Gupta and R.F. Laubscher, Sustainable Machining of Titanium Alloys: A Critical Review, *Proc. Inst. Mech. Eng.*, 2017, **231**(14), p 2543–2560
8. T.D. Popovici and I. Ciocan, Experimental Study on Cutting Forces at Ti6Al4V Milling, *Adv. Mater. Res.*, 2015, **1128**, p 288–292
9. C.R.F. Azevedo, D. Rodrigues, and F.B. Neto, Ti-Al-V Powder Metallurgy (pm) via the Hydrogenation–Dehydrogenation (hdh) Process, *J. Alloys Compd.*, 2003, **353**(1), p 217–227

10. B. Sharma, S.K. Vajpai, and K. Ameyama, Microstructure and Properties of Beta Ti-Nb Alloy Prepared By Powder Metallurgy Route Using Titanium Hydride Powder, *J. Alloys Compd.*, 2012, **656**, p 978–986
11. A.T. Sidambea, I.A. Figueroaa, H.G.C. Hamiltonb, and I. Todda, Metal Injection Moulding of CP-Ti Components for Biomedical Applications, *J. Mater. Process. Technol.*, 2012, **212**(7), p 1591–1597
12. P. Perssona, A.E.W. Jarforsb, and S. Savagec, Self-Propagating High-Temperature Synthesis and Liquid-Phase Sintering of TiC/Fe Composites, *J. Mater. Process. Technol.*, 2011, **127**(2), p 131–139
13. X.X. Ye, B. Chen, J.H. Shen, J. Umeda, and K. Kondoh, Microstructure and Strengthening Mechanism of Ultrastrong and Ductile Ti-xSn Alloy Processed by Powder Metallurgy, *J. Alloys Compd.*, 2017, **709**(30), p 381–393
14. D.G. Savvakin, A. Carman, O.M. Ivasishin, M.V. Matviychuk, A.A. Gazder, and E.V. Pereloma, Effect of Iron Content on Sintering Behavior of Ti-V-Fe-Al near-β Titanium Alloy, *Metall. Mater. Trans. A*, 2012, **43**(2), p 716–723
15. L. Bolzoni, E. Herraiz, E.M. Ruiz-Navas, and E. Gordo, Study of the Properties of Low-Cost Powder Metallurgy Titanium Alloys by 430 Stainless Steel Addition, *Mater. Des.*, 2014, **60**(8), p 628–636
16. C.J. Bettles, S. Tochon, M.A. Gibson, B.A. Welk, and H.L. Fraser, Microstructure and Mechanical Properties of Titanium Aluminide Compositions Containing Fe, *Mater. Sci. Eng. A*, 2013, **575**(6A), p 152–159
17. L. Bolzonia, E.M. Ruiz-Navasb, and E. Gordob, Quantifying the Properties of Low-Cost Powder Metallurgy Titanium Alloys, *Mater. Sci. Eng. A*, 2017, **687**, p 47–53
18. R. Licheri, R. Orrù, and G. Cao, Chemically-Activated Combustion Synthesis of TiC-Ti Composites, *Mater. Sci. Eng. A*, 2004, **367**(1), p 185–197
19. V.A. Popov, M. Burghammer, M. Rosenthal, and A. Kotov, In Situ Synthesis of TiC Nano-Reinforcements in Aluminum Matrix Composites During Mechanical Alloying, *Composites Part B*, 2018, **145**, p 57–61
20. B. AlMangour, D. Grzesiak, and J. Yang, In-situ Formation of Novel TiC-Particle-Reinforced 316L Stainless Steel Bulk-Form Composites By Selective Laser Melting, *J. Alloys Compd.*, 2017, **706**, p 409–418
21. X. Yuan, G. Liu, H. Jin, and K. Chen, In Situ Synthesis of TiC Reinforced Metal Matrix Composite (MMC) Coating By Self-Propagating High Temperature Synthesis (SHS), *J. Alloys Compd.*, 2011, **509**(30), p 301–303
22. Standard E8, Standard test methods for tension testing of metallic materials, 2004
23. G.A. Salishchev, S.V. Zerebtsov, S.Y. Mironov, and S.L. Semiatin, Formation of Grain Boundary Misorientation Spectrum in Alpha-Beta Titanium Alloys with Lamellar Structure Under Warm and Hot Working, *Mater. Sci. Forum*, 2004, **467–470**, p 501–506
24. J.L. Murray, *Phase Diagrams of Binary Titanium Alloys*, ASM International, Metals Park, Ohio, 1987
25. H. Nakajima, K. Ogasawara, S. Yamaguchi, and M. Koiwa, Diffusion of Chromium in α-Titanium and its Alloys, *Mater. Trans. JIM*, 1990, **1**(4), p 249–254
26. D.B. Lee, K.B. Park, H.W. Jeong, and S.E. Kim, Mechanical and Oxidation Properties of Ti-xFe-ySi Alloys, *Mater. Sci. Eng. A*, 2002, **328**(1), p 161–168
27. J. Jiang, S. Li, W. Zhang, W. Yu, and Y. Zhou, In Situ Formed TiCx in High Chromium White Iron Composites: Formation Mechanism and Influencing Factors, *J. Alloys Compd.*, 2019, **788**, p 873–880
28. B. AlMangour, D. Grzesiak, and J. Yang, In situ Formation of TiC-Particle-Reinforced Stainless Steel Matrix Nanocomposites During Ball Milling: Feedstock Powder Preparation for Selective Laser Melting at Various Energy Densities, *Powder Technol*, 2018, **326**, p 467–478
29. ASTM standard B367, Specification for titanium and titanium alloy castings, 2013